

Multiple signatures of topological transitions for interacting fermions in chain lattices

Y.-H. Chan

Institute of Atomic and Molecular Sciences, Academia Sinica, Taipei 10617, Taiwan

Ching-Kai Chiu

Department of Physics and Astronomy, University of British Columbia, Vancouver, British Columbia, Canada V6T 1Z1

Kuei Sun*

Department of Physics, The University of Texas at Dallas, Richardson, Texas 75080-3021, USA

We study one-component fermions in chain lattices with proximity-induced superconducting gap and interparticle short-range interaction, capable of hosting Majorana fermions. By systematically tracking various physical quantities, we show that topological states and topological phase transitions in the system can be identified by multiple signatures in thermodynamic quantities and pair-condensate properties, in good agreement with the known signatures in the ground-state energy and entanglement spectrum. We find the disappearance of the topological phase in a largely attractive regime, in which the system undergoes a first-order transition between two topologically trivial states. In addition, the stability of the signatures against finite size, disorder, and inhomogeneity is analyzed. Our results provide additional degrees of freedom for the characterization of topological states with interaction and for the experimental detection of emergent Majorana fermions.

PACS numbers: 74.20.-z, 03.65.Vf, 74.78.Na, 71.10.Fd

I. INTRODUCTION

Exploring topological states of matter has become a rapidly developing field in condensed matter physics [1–3]. One intriguing topological state that exhibits both fundamental interest and practical application is the emergent Majorana zero modes or Majorana fermions [4–8], which are their own antiparticles and possess zero energy, in superconducting materials. The pursuit of the Majorana modes started from the study of a one-dimensional (1D) p -wave superconducting chain by Kitaev [9]. This milestone has triggered several alternative schemes for the realization of Majorana fermions, such as $p + ip$ superconductors [10–14], spin-orbit coupled superconducting nanowires [15–18], chains of magnetic atoms on superconducting substrates [19–22], superconducting surfaces of topological insulators [23–26], superfluid helium 3 [27–29], and ultracold atoms [30–35]. Recently, a semiconductor nanowire with intrinsic spin-orbit coupling, external magnetic field, and proximity-induced superconductivity has become one of the experimentally promising platforms to host Majorana fermions [36–41], which appear on the edges of the wire and lead to a tunneling conductance peak at zero voltage. Such a zero-bias peak has been observed as (indirect) evidence for their existence.

In addition to the transport properties [42–54], searching different signatures for the topological phase is an ongoing task for the investigation of Majorana fermions. From the experimental point of view, it not only provides more evidence for direct detection of Majorana fermions but also helps rule out different physical causes

that result in the same transport behavior [55–58]. From the theoretical point of view, a comparison between various quantities, even those typically used to describe Ginzburg-Landau-type phase transitions, such as susceptibilities and superfluid order, can provide useful information for characterizing topological phases and topological phase transitions, especially in interacting systems [59–61]. Interaction effects, which are unavoidably present in reality, may alter physical features of the topological phase and even change the topology [59–71]. For example, time-reversal symmetric Kitaev chains in class BDI change the topological invariant from \mathbb{Z} to \mathbb{Z}_8 when the interaction is turned on [71]. In an interacting system, Majorana zero modes at edges become many-body Majorana wave functions [72, 73] and the degenerate ground states with two different parities are connected by these many-body Majorana zero operators. Such many-body phenomena attract broad interest, from the fundamental understanding of its nature to applications on quantum computation [74–77]. The study of multiple signatures shall provide a convincing series of tests to characterize the interacting topological phase diagram. Recent works have analyzed individual quantities for separate models, such as entanglement spectrum in a spin-orbit coupled chain with interactions [62, 66], compressibility [78] and spectral function [63] in the Kitaev chain, as well as susceptibility [65] and pair correlation [59] in long-range coupled superconducting fermions. However, these works have not provided a systematic comparison of multiple quantities between topological/trivial phases or upon topological transitions within a single frame (model).

In this paper, we study various physical quantities of 1D one-component fermions having proximity-induced pairing gap and interparticle short-range interaction, as a generalization of the Kitaev model. These quantities

* Corresponding author. kuei.sun@utdallas.edu

are obtained from density-matrix-renormalization-group (DMRG) [79, 80] calculations and categorized into three groups: (i) topological properties, including ground-state degeneracy and entanglement spectrum; (ii) thermodynamic properties, including compressibility and susceptibility; and (iii) condensate properties, including pair-condensate fraction and Cooper-pair size. We take the topological region indicated by the first group as a reference and investigate the behavior of the second and third ones in the parameter space. As a result, we shall find alternative signatures to identify the topological states and topological transitions. In addition, by tracking the multiple signatures, we show the topological phase diagram as a function of interaction. Finally, we study the behavior of several signatures against finite size, disorder, as well as inhomogeneity, and discuss their stability under these conditions.

The paper is organized as follows. In Sec. II, we introduce the model Hamiltonian and define the physical quantities of interest. Section III shows the setup of DMRG calculations. We present the results and discussions in Sec. IV. Section V is the conclusion.

II. MODEL AND PHYSICAL QUANTITIES

In this section, we present the model in consideration and physical quantities of interest. We consider one-component fermions in chain lattices where particles can scatter through the Cooper channel (or form Cooper pairs) due to a combined effect of external proximity-induced pairing and internal short-range interaction. If there is only the external effect, the Hamiltonian is of the Kitaev form [9],

$$H_K = H_0 + \sum_{j=1}^{L-1} \left(\Delta' \hat{c}_{j+1}^\dagger \hat{c}_j^\dagger + \text{H.c.} \right), \quad (1)$$

where \hat{c}_j^\dagger creates a fermion on site j , Δ' (taken real without the loss of generality) describes the proximity-induced pairing, L is the total number of lattice sites, and

$$H_0 = \sum_{j=1}^{L-1} -t \left(\hat{c}_j^\dagger \hat{c}_{j+1} + \text{H.c.} \right) - \mu \sum_{j=1}^L \hat{n}_j \quad (2)$$

is the noninteracting Hamiltonian with number operator $\hat{n}_j = \hat{c}_j^\dagger \hat{c}_j$, nearest-neighbor tunneling t , and chemical potential μ . If there is only the internal interaction effect, the Hamiltonian reads

$$H_I = H_0 + \sum_{j=1}^{L-1} V' \hat{n}_j \hat{n}_{j+1}, \quad (3)$$

where negative (positive) V' represents attractive (repulsive) interaction. In realistic cases of a nanowire [36–41] or an atomic chain [19–21] on a superconducting substrate, or a tube of quantum gases in higher-dimensional optical lattices [35], both effects can take place. We hence

model the system with a phenomenological parameter γ to describe the relative strength of the two effects and write down our model Hamiltonian,

$$H = (1 - \gamma)H_K + \gamma H_I \\ = H_0 + \sum_{j=1}^{L-1} \Delta \left(\hat{c}_{j+1}^\dagger \hat{c}_j^\dagger + \text{H.c.} \right) + V \hat{n}_j \hat{n}_{j+1}, \quad (4)$$

with independent variables $\Delta = (1 - \gamma)\Delta'$ and $V = \gamma V'$, which can be self-consistently determined by microscopic degrees of freedom and/or realistic parameters of the system. (Below we aim to study physical characteristics of H in a range of its parameter space rather than determine the parameters for a specific situation.) The Hamiltonian always conserves the even/odd parity of total number of particles $N = \langle \hat{N} \rangle = \langle \sum \hat{n}_j \rangle$ due to $[H, (-1)^{\hat{N}}] = 0$ and conserves N (meaning $[H, \hat{N}] = 0$) in the limit $\Delta \rightarrow 0$.

We will study the behavior of three groups of physical quantities of interest in the topological and non-topological regions as well as upon the topological transition. The first group, called topological quantities, includes ground-state degeneracy and entanglement spectrum degeneracy. The former one can be characterized by the energy difference

$$\delta E = |E_{\text{even}} - E_{\text{odd}}| \quad (5)$$

between the lowest eigen energies $E_{\text{even/odd}}$ of the even and odd blocks of the Hamiltonian [where $\langle (-1)^{\hat{N}} \rangle_{\text{even/odd}} = \pm 1$], respectively. The ground-state degeneracy $\delta E = 0$ occurs as the manifestation of Majorana fermions in the topological region and does not otherwise.

The entanglement spectrum is a series of eigenvalues of reduced density matrix ρ_R obtained by tracing out half spatial degrees of freedom of the ground-state wave function $|\psi_g\rangle$,

$$\rho_R = \text{Tr}_{j \leq L/2} |\psi_g\rangle \langle \psi_g|, \quad (6)$$

where we consider L an even number and choose the ground state of the even-particle-number block when the even-odd degeneracy occurs ($\delta E = 0$). We obtain a set of $2N_\lambda$ largest eigenvalues of ρ_R , denoted by $\{\lambda_j\}$ and sorted as $\lambda_j \geq \lambda_k$ if $j < k$, and compute the difference between paired elements defined by

$$\delta \lambda \equiv \sum_{j=1}^{N_\lambda} |\lambda_{2j-1} - \lambda_{2j}|. \quad (7)$$

Given sufficiently large N_λ , the condition $\delta \lambda \rightarrow 0$ guarantees twofold degeneracy in the entanglement spectrum, which is contributed by a pair of Majorana fermions separated in each entanglement subsystem and hence regarded as a signature for their existence (see details in Refs. [81–83]).

The second group involves thermodynamic quantities that can be expressed as the derivative of energy density

$E = \langle H \rangle / L$ with respect to the system parameters. We focus on the first derivative $-\frac{\partial E}{\partial \mu}$, which is equal to the particle density $\rho = N/L$ from the Hellmann-Feynman theorem, and second derivatives $-\frac{\partial^2 E}{\partial X \partial Y}$, which describe compressibility ($X = Y = \mu$) or various susceptibility ($X = Y = \Delta$ or $X = \mu, Y = \Delta$) of the system. A discontinuity or a peak of energy derivatives represents a drastic change in the behavior of the ground-state energy, which implies a cross between two lowest-energy states of the system. Such a cross is a necessary condition for a topological transition.

The third group includes quantities describing condensate properties. Superconducting fermions can be considered as a pair condensate in which a two-body or Cooper-pair state is macroscopically occupied [84, 85], analogous to the Bose-Einstein condensation in bosonic systems [86, 87]. The condensate properties are well characterized by the pair density matrix ρ^{pair} , whose element is defined in spatial coordinates as

$$\rho_{jk;j'k'}^{\text{pair}} = \langle c_j^\dagger c_k^\dagger c_{k'} c_{j'} \rangle. \quad (8)$$

When the condensation occurs, ρ^{pair} has an eigenvalue $\lambda_0^{\text{pair}} [\sim O(N)]$ largely compared to the others $[\sim O(1)]$, representing the macroscopic occupation or the number of condensed pairs. This number defines the condensate fraction as

$$P = \frac{\lambda_0^{\text{pair}} - 2}{N}, \quad (9)$$

with an offset 2 of the noninteracting limit [60] [such that $P = 0$ for a free system described by H_0 in Eq. (2)]. The eigenstate ψ_{jk}^{pair} corresponding to λ_0^{pair} represents the Cooper-pair wave function. The Cooper-pair size is defined as a root-mean-square distance between the two particles in a pair,

$$r_{\text{pair}} = \sqrt{\sum_{j,k} (j-k)^2 |\psi_{jk}^{\text{pair}}|^2}, \quad (10)$$

and indicates a length scale over which two fermions bind in real space. The topological state is a weak-pairing state [88] with $r_{\text{pair}} \rightarrow \infty$ (or $\sim L$ in a finite-size system), which originates the long-range entangled Majorana fermions on both ends. Instead, the trivial state has finite r_{pair} (or $\ll L$). Therefore, a drastic change in r_{pair} is expectable upon the topological transition. Note that the commonly used $U(1)$ symmetry-breaking order [6] can distinguish the weak-pairing state (being constant, corresponding to an infinite Cooper-pair size) from the strong-pairing one (exponentially decaying in real space, with the decay rate determining a finite Cooper-pair size) for a number-nonconserving state, but fails to do so with a number-conserving one (e.g., $\Delta \rightarrow 0$ in our model). The definition of r_{pair} in Eq. (10) works for both. (In fact, such r_{pair} has been applied to study topological properties in a two-dimensional system [59].)

We have shown the model Hamiltonian and all of the physical quantities of interest. Among these quantities, twofold degeneracies of ground-state energy and entanglement spectrum can be regarded as direct signatures for the topological states and Majorana fermions. They have also been proved for interacting systems [62, 82]. A large Cooper-pair size is directly related to the long-range entanglement for the presence of Majorana fermions, while the interaction effects on it are to be investigated. The energy derivatives such as compressibility and susceptibility can imply a cross of the two lowest-energy states, but its relation to the topological phase transition needs to be confirmed by the comparison with the direct signatures. Below we will take the ground-state energy and entanglement spectrum as a reference to pinpoint other signatures displayed in the thermodynamic quantities and/or condensate properties. In the next two sections, we present the numerical setup, results, and discussions.

III. NUMERICAL SETUP

While exact solutions can be found in specific parameter regions [89], the many-body ground state of the interacting Hamiltonian in Eq. (4) can, in general, be computed numerically. Our numerical results are obtained using the DMRG [79, 80] method, whose accuracy has been demonstrated in computing the ground-state properties of a short-range coupled 1D system. This method has been widely adopted to study topological properties in spinless fermions [63, 90], spin-orbit coupled electrons [62, 66, 67], and ultracold atoms [91, 92]. In our work, we employ the DMRG method on systems up to $L = 256$. The Z_2 symmetry of parity conservation is considered to reduce the computational cost. We keep up to $m = 120$ states and apply seven sweeps in the ground-state calculation. The number of states m kept in the DMRG method determines the size of the approximated Hamiltonian and hence the accuracy of calculations. The discarded weight in the eigenvalue of the reduced density matrix with $m = 120$ is of the order of 10^{-8} , which guarantees the convergence of the ground-state properties.

The DMRG calculations are numerically efficient for obtaining the ground-state energy, entanglement spectrum, and real-space two-point correlations. However, the bottleneck of our numerical study lies in the computation of the condensate properties. The construction of the pair density matrix requires the evaluation of all possible four-point correlations. Due to the L^4 -growing computational cost as the system size increases, we are bounded to $L = 64$. Another limit is the diagonalization of the pair density matrix, whose computational effort scales as L^8 and will eventually dominate in a large-size case.

IV. RESULTS

In this section, we present and discuss results that track multiple quantities for several cases of interest.

We take the tunneling strength t to be the energy units for convenience and set $\Delta = 0.2$. First, we study the well-known Kitaev chain (where the internal interaction $V' = 0$) and find the compressibility and susceptibility as good signatures for the topological transition. Second, we track the compressibility for general cases with the internal interaction. We will show that it remains a valid indicator because it indicates the same topological region as the entanglement spectrum does. Third, we investigate the condensate properties together with the compressibility as topological signatures for a relatively small system. We also study the characterization of topological phases with the use of number density and condensed-pair density. Finally, we present the effects of finite size, disorder, and inhomogeneity.

A. The Kitaev model

The Kitaev chain model is described by the Hamiltonian of Eq. (1). It also represents the weakly interacting limit $V \rightarrow 0$ of our model Hamiltonian of Eq. (4). The upper and lower topological transition points of an infinite Kitaev chain are known as $\mu = \pm 2 \equiv \mu_c^\pm$ [9], between (outside) which the system is in a topological (trivial) state. For a finite chain, we numerically calculate the transition points. They show little change if the system size is large compared with the characteristic size of Majorana fermions.

Figure 1 shows four thermodynamic quantities as energy derivatives: density $\rho = -\frac{\partial E}{\partial \mu}$ [Fig. 1(a)], compressibility $\frac{\partial \rho}{\partial \mu} = -\frac{\partial^2 E}{\partial \mu^2}$ [Fig. 1(b)], and susceptibilities $-\frac{\partial^2 E}{\partial \Delta^2}$ [Fig. 1(c)] as well as $-\frac{\partial^2 E}{\partial \Delta \partial \mu}$ [Fig. 1(d)], vs the chemical potential μ . We plot data for an infinite chain (solid curve) and a finite chain of $L = 256$ with open (red crosses), periodic (blue circles), and antiperiodic (green triangles) boundary conditions. We see that the density smoothly varies from vacuum ($\rho = 0$) to commensurate filling ($\rho = 1$) as μ increases. The trivial states have either a very low filling ($\rho \sim 0$ in $\mu < \mu_c^-$) or an almost commensurate filling ($\rho \sim 1$ in $\mu > \mu_c^+$). All of the second derivatives of the energy develop peaks at each transition point. The compressibility peaks reflect the bulk gap closing at the transition point [78]. Across the peak, a sign change of the curve slope indicates a discontinuity in the third derivative of energy, which implies that the topological transition is third order. Such a topological transition type has also been found in a long-range coupled system [65]. The peak structure is independent of the chain size (see more analyses in Sec. IV D) as well as the boundary conditions and can thus be taken as a reliable signature for the topological transition. While the two susceptibilities both ought to work well, below we study the compressibility, i.e., a typical observable in experiments, as an indicator for cases with internal interaction.

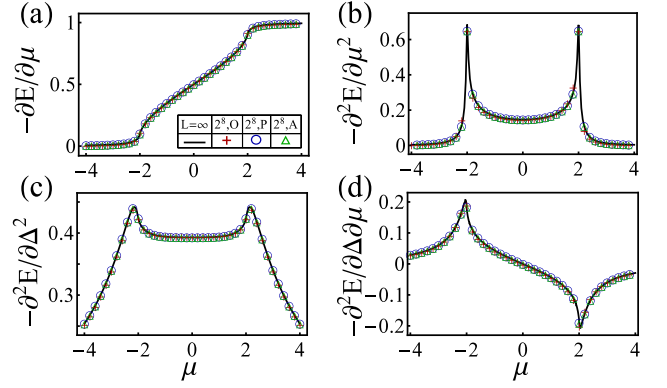


FIG. 1. (Color online) Noninteracting system energy's (a) first derivative $-\frac{\partial E}{\partial \mu} = \rho$ and various second derivatives (b) $-\frac{\partial^2 E}{\partial \mu^2} = \frac{\partial \rho}{\partial \mu}$, (c) $-\frac{\partial^2 E}{\partial \Delta^2}$, and (d) $-\frac{\partial^2 E}{\partial \Delta \partial \mu} = \frac{\partial \rho}{\partial \Delta}$, vs chemical potential μ . Four cases of $L = \infty$ (solid curve) and $L = 256$ with open (red crosses), periodic (blue circles), and antiperiodic (green triangles) boundary conditions are presented. The superconducting gap is set as $\Delta = 0.2$.

B. Effects of internal interaction

With the internal interaction turned on ($V \neq 0$), we calculate the ground state properties as a function of V for a case of $L = 256$. In Fig. 2(a), we plot compressibility $\frac{\partial \rho}{\partial \mu}$ vs chemical potential μ at various $V = -0.4$ (purple diamonds), -0.2 (blue circles), 0 (green triangles), 0.2 (yellow squares), and 0.4 (red crosses). The curves maintain the two-peak structure, while the right transition point μ_c^+ has a positive (negative) shift at repulsive (attractive) internal interaction, and the left one μ_c^- shows little change with the interaction. We also confirm that the region sandwiched by the compressibility peaks coincides with the topological region identified by the ground-state degeneracy and entanglement spectrum. Therefore, compressibility can be regarded as a reliable signature for topological states of interacting systems. Figure 2(b) shows compressibility vs density ρ in the same convention as Fig. 2(a). Similarly, the curves display peaks at the two transition points. We notice that the position of the left (right) peak is at a low (high) filling, $\rho < 0.1$ (> 0.9), and is insensitive to interaction. In other words, the topological state survives in most intermediate-filling regions, which promises the Majorana fermions in a wide range of density-controllable systems such as ultracold atoms.

Since the topological region shrinks as the interaction becomes more attractive, we turn to study the fate of the topological state in the strongly attractive region. (Note that the strongly repulsive region has been well studied in Ref. [63].) The top panel of Fig. 2(c) shows compressibility vs μ at $V = -1.5$ (red crosses), -2 (green triangles), and -2.5 (blue circles), with the topological region shaded. We see that the two peaks at μ_c^\pm merge into one at $V = -2.5$ and the topological region disappears. The disappearance can also be seen in the entanglement spec-

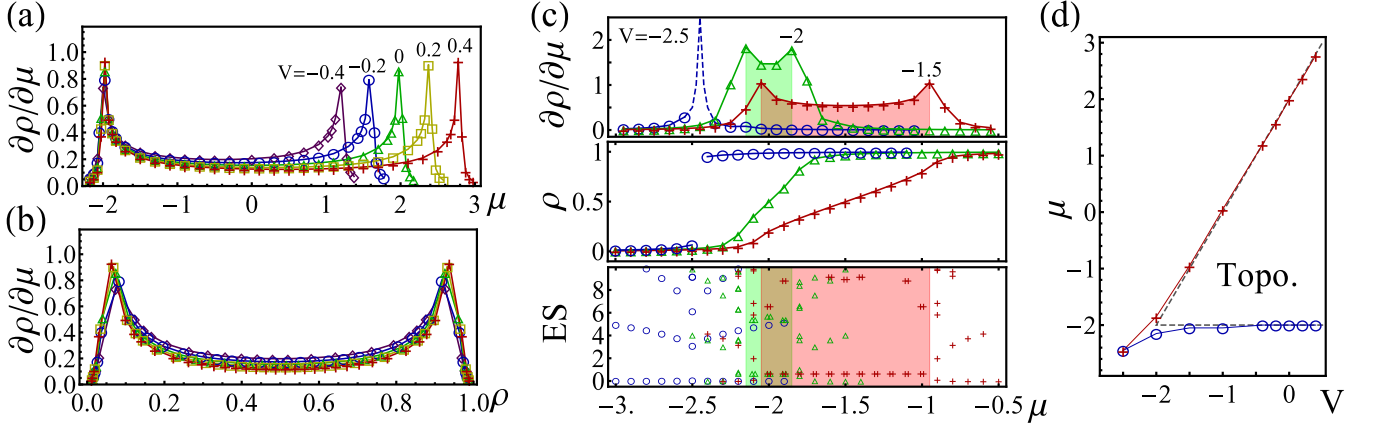


FIG. 2. (Color online) (a),(b) Compressibility $\frac{\partial\rho}{\partial\mu}$ vs μ and ρ , respectively, at various interactions $V = -0.4$ (purple diamonds), -0.2 (blue circles), 0 (green triangles), 0.2 (yellow squares), and 0.4 (red crosses) for an open chain of $L = 256$ and $\Delta = 0.2$. (c) $\frac{\partial\rho}{\partial\mu}$ (top panel), ρ (middle panel), and entanglement spectrum (ES, bottom panel) vs μ at relatively large attraction $V = -1.5$ (red crosses), -2 (green triangles), and -2.5 (blue circles). The topological region for each V is shaded in the top and bottom panels for comparison. The dashed curve in the top panel shows how the two compressibility peaks would emerge at $V = -2.5$, although the actual value is undefined due to the discontinuity in ρ . (d) Interacting phase diagram showing the topological region in the V - μ plane. The upper and lower boundaries are marked by red crosses and blue circles, respectively, while the dashed curve shows the Hartree mean-field results.

trum in the bottom panel as the doubly degenerate region vanishes at $V = -2.5$. The density curves in the middle panel show that the topological transitions at $V = -1.5$ and -2 still happen at either a low or high filling. When the topological region disappears at $V = -2.5$, the density ($= -\frac{\partial E}{\partial\mu}$) curve exhibits a discontinuity and the system undergoes a first-order transition between a trivial low-filling state and a trivial high-filling one.

The phase boundary shift can be explained by an effective chemical-potential shift due to the interaction. Considering a Hartree approximation $n_{j+1}n_j \rightarrow \rho n_j + \rho n_{j+1} - \rho^2$, one can turn the Hamiltonian of Eq. (4) into the original Kitaev form with an effective chemical potential $\mu_{\text{eff}} = \mu - 2V\rho$, where $\rho = \rho(\mu, V)$. The upper and lower transition points are thus given by $\mu_{\text{eff}} = \pm 2$, respectively, which leads to

$$\mu_c^\pm = \pm 2 + 2V\rho(\mu_c^\pm, V). \quad (11)$$

Because the density at the lower (upper) transition point is low (high) and insensitive to interaction, we approximately insert $\rho(\mu_c^-, V) = 0$ and $\rho(\mu_c^+, V) = 1$ into Eq. (11) and obtain $\mu_c^+ = 2 + 2V$ and $\mu_c^- = -2$. Such relations tell that the lower boundary barely depends on V and the upper boundary linearly shifts with V . Figure 2(c) shows the topological region in the V - μ plane. The upper and lower phase boundaries from this approximation (dashed curves) well match those from the numerical calculations (red crosses and blue circles, respectively).

C. Condensate properties

In this section, we study pair-condensate properties of the system. As mentioned in Sec. III, the calculation of the pair density matrix can be time consuming. Such

a constraint directs our focus on a relatively small system ($L = 32$) rather than a large one. The top panel of Fig. 3 shows the compressibility curves as a reference for the topological region at various interactions [conventions are the same as in Fig. 2(a)]. The middle and bottom panels show the condensate fraction P defined in Eq. (9) and Cooper-pair size r_{pair} defined in Eq. (10),

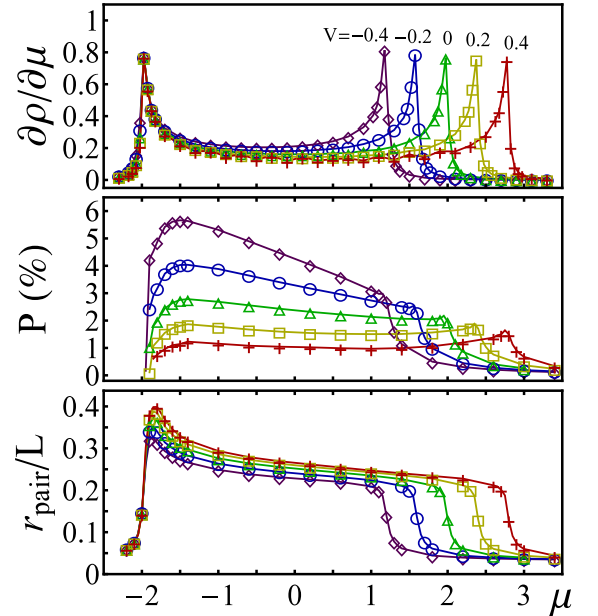


FIG. 3. (Color online) Compressibility $\frac{\partial\rho}{\partial\mu}$ (top panel), condensate fraction P (middle panel), and Cooper-pair size r_{pair} (bottom panel) vs μ at various interactions for an open chain of $L = 32$ and $\Delta = 0.2$. Conventions are the same as in Fig. 2(a).

respectively. Different from the compressibility and entanglement spectrum, we first see that the curves of condensate properties lack symmetry with respect to the half-filling point. At the upper phase boundary (right peak of the compressibility curve) both P and r_{pair} develop a kink, indicating a sudden change in the condensate properties upon the topological transition. The sharp decrease of r_{pair} is consistent with the transition from weak-pairing (topological) to strong-pairing (trivial) states [6, 88]. At the lower boundary (left peak of the compressibility curve), r_{pair} shows a peak, while P changes the trend but does not show a clear signature due to the finite-size effect (the filling is so low such that the total number of particles is smaller than two). We increase the system size and find that the turning point of P approaches the phase boundary. Therefore, the behavior of P and r_{pair} can be an indicator for the topological transition.

The topological transition accompanied by a significant change in the Cooper-pair size raises an interesting question of whether the change in the pair condensate can be purely qualitative or must be both qualitative and quantitative. We try to answer this question by examining two essential quantities of a pair condensate, i.e., the total number of particles N and the total number of condensed pairs λ_0^{pair} , around the topological phase boundary. The answer is the former if the system can go across the phase boundary and keep both N and λ_0^{pair} unchanged (only r_{pair} changes). Our model is suited to explore this question because it is defined in a three-dimensional parameter space (Δ, V, μ) such that a path along which two functions $N(\Delta, V, \mu)$ and $\lambda_0^{\text{pair}}(\Delta, V, \mu)$ remain constant becomes mathematically possible. We explore large enough regions around upper and lower transition points, $(\Delta, V, \mu) = (0.2, 0, \pm 2)$, respectively, by varying all three parameters for a $L = 64$ case. The results show that one of N and λ_0^{pair} can remain constant upon the topological transition, but not both. In other words, the topological transition or the sudden change of the Cooper-pair size in our model can be regarded as a result of a quantitative change in N or λ_0^{pair} . Moreover, we do not find that a topological state and a trivial state have the same N and λ_0^{pair} . Our results may have implications for the characterization of topological states by $(N/L, \lambda_0^{\text{pair}}/L)$.

We further study this possibility by computing the condensate properties for hundreds of points in the range of $0.15 \leq \Delta \leq 0.45$, $-0.45 \leq V \leq 0.4$, and $1.4 \leq \mu \leq 3.4$, for $L = 32$. Figure 4 shows the data points representing three different ranges of the Cooper-pair size around the upper topological transition region in the plane of N/L and $\lambda_0^{\text{pair}}/L$. The system can be considered as a topological state if $r_{\text{pair}} \geq 4$. We see that along a vertical (horizontal) path in Fig. 4, the system can undergo a topological transition at fixed N (λ_0^{pair}). On the other hand, the concurrence of a decrease in r_{pair} and an increase in either N or λ_0^{pair} confirms our conjecture, i.e., an inevitable quantitative change upon the topological

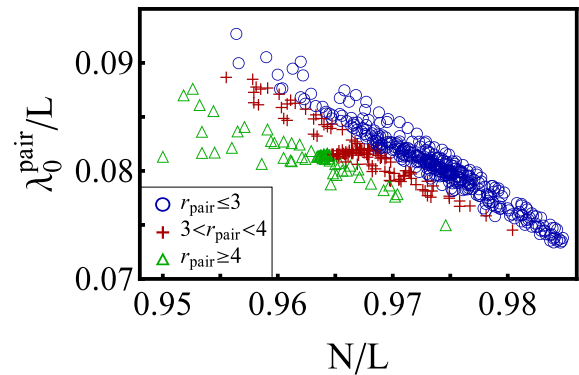


FIG. 4. (Color online) Data points showing three different ranges of the Cooper-pair size, i.e., $r_{\text{pair}} \leq 3$ (blue circles), $3 < r_{\text{pair}} < 4$ (red crosses), and $r_{\text{pair}} \geq 4$ (green triangles), in the plane of N/L and $\lambda_0^{\text{pair}}/L$ for $L = 32$.

transition. In other words, r_{pair} is a function of N and λ_0^{pair} , and these two parameters can hence be used to characterize the topological phase diagram. We finally comment that a more solid confirmation lies in the convergence of Fig. 4 in the thermodynamic limit; we leave the test of this for future study once more powerful computational tools are available.

D. Effects of finite size, disorder, and inhomogeneity

In the last section, we explore the stability of the signatures against three realistic effects in experiments—finite size, disorder, and inhomogeneity. Figure 5 shows the compressibility (top panel), energy difference δE (middle panel) defined in Eq. (5), and entanglement spectrum difference $\delta \lambda$ (bottom panel) defined in Eq. (7) vs μ for $L = 32$ (red crosses), 48 (blue circles), and 64 (green triangles). We see that although all three quantities indicate the transition points, the compressibility curve is insensitive to the system size, while δE and $\delta \lambda$ can increase by several orders as the system size is halved. Therefore, the compressibility is a stable indicator against the finite-size effect. The insensitivity also provides a more numerically efficient way to predict the topological transition of a large-size system by calculating the compressibility peak of a relatively small one.

For the disorder effect, we consider a Hamiltonian

$$H_d = H + \sum_{j=1}^L \delta_j \hat{n}_j, \quad (12)$$

with a set of random local potential shifts $\{\delta_j\}$ that obey the normal distribution and have zero average. For the inhomogeneous effect, we consider an external harmonic trap with curvature K turned on,

$$H_t = H + \sum_{j=1}^L \frac{K}{2} \left(j - \frac{L}{2} - \frac{1}{2} \right)^2 \hat{n}_j. \quad (13)$$

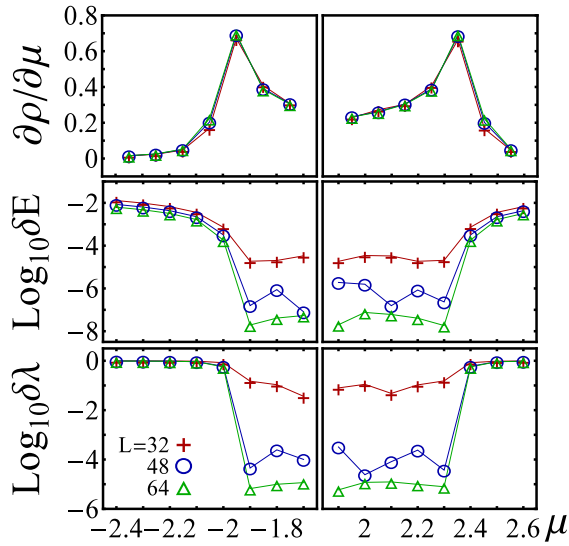


FIG. 5. (Color online) Compressibility $\frac{\partial \rho}{\partial \mu}$ (top panel), energy gap between the ground state and first excited state δE (middle panel), and difference between even and odd sectors of entanglement spectrum $\delta \lambda$ (bottom panel) vs μ around the lower (left column) and upper (right column) transition points at various open-chain sizes: $L = 32$ (red crosses), 48 (blue circles), and 64 (green triangles), respectively. Data are for $\Delta = V = 0.2$.

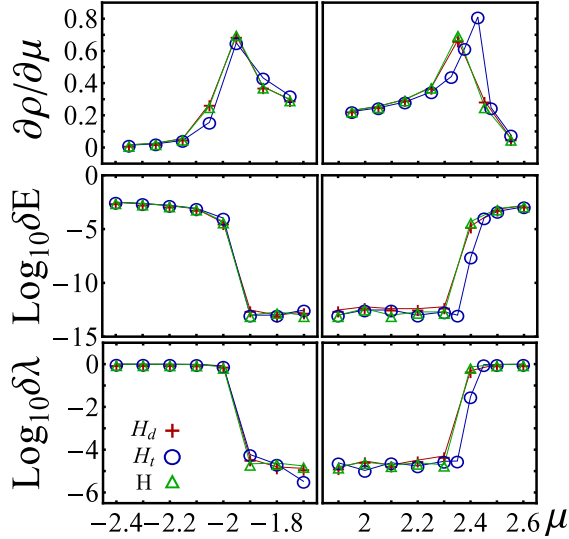


FIG. 6. (Color online) Comparison between a disorder system [H_d of Eq. (12), red crosses], a trap system [H_t of Eq. (13), blue circles], and a reference without these effects [H of Eq. (4), green triangles]. Conventions are the same as in Fig. 5, except the system size here is $L = 128$.

In Fig. 6, we compare a disorder case (red crosses) with the variance of $\{\delta_j\}$ equal to 0.1 and a trap case (blue circles) with $K = 0.8/(L-1)^2$ with the original Hamiltonian H for $L = 128$ in the same convention of Fig. 5. We see

that neither of the two effects can alter the signatures for the topological transition. Such results are anticipated because the topological states and Majorana fermions are symmetry protected. Perturbations can not destroy the topological order as long as they are not strong enough to cause the bulk-gap crossing. (Regimes of strong disorder or deep traps are beyond the scope of this study. One could refer to previous works in Refs. [34, 93–96].)

V. CONCLUSION

In conclusion, multiple physical quantities have been analyzed for one-component fermions with proximity-induced superconducting gap and interparticle interaction in 1D lattices, which can be a topological superconductor hosting Majorana fermions. In addition to the double degeneracy of ground-state energy and entanglement spectrum, we have found that the topological transition can also be revealed by peaks of compressibility and susceptibility curves, as well as a sudden change of trend in the condensate fraction and Cooper-pair size. Among them, the compressibility peak is particularly useful for its stability against the finite-size effect and being observable in experiments. The Cooper-pair size directly shows the topological transition between strong-pairing and weak-pairing states. By tracking these signatures, we have found that the topological transition is third order. As the interaction becomes more attractive, the topological state finally disappears and the system undergoes a first-order transition between low-filling and high-filling trivial states. We have also explored the possibility to characterize the topological phase using density of particles and that of condensed pairs. One future direction is the extension of this study to other interacting platforms in which various tunneling or pairing channels [60, 97, 98] need to be considered and an alternative treatment suited for the continuous space [99, 100] may apply. In addition, our results may find applications on spin systems that are associated with our Hamiltonian of Eq. (4), such as an Ising chain with a transverse field ($V \rightarrow 0$, e.g., see Ref. [101]), the XXZ model ($\Delta \rightarrow 0$) [102], the Baxter XYZ model ($\mu \rightarrow 0$) [103], and the two-dimensional classical Ising model ($V \rightarrow 0$, $t = \Delta$) [104].

Acknowledgements: We are grateful to J. Alicea, C. J. Bolech, L. Duan, M. Franz, T. L. Hughes, H.-H. Hung, A. J. Leggett, J. H. H. Perk, N. Shah, and C. Zhang for informative discussions. Y.H.C. acknowledges the support by the Thematic Project at Academia Sinica. C.K.C. gratefully acknowledges the support of the Max-Planck-UBC Center for Quantum Materials. K.S. is supported by ARO (Grant No. W911NF-12-1-0334) and AFOSR (Grant No. FA9550-13-1-0045). Part of the numerical work was developed using the DMRG code released within the Powder with Power project (<http://qti.sns.it/dmrg/>). We acknowledge the computational resource provided by University of Cincinnati and Texas Advanced Computing Center (TACC).

[1] M. Z. Hasan and C. L. Kane, Colloquium: Topological insulators, *Rev. Mod. Phys.* **82**, 3045 (2010).

[2] X.-L. Qi and S.-C. Zhang, Topological insulators and

- superconductors, *Rev. Mod. Phys.* **83**, 1057 (2011).
- [3] C.-K. Chiu, J. C. Y. Teo, A. P. Schnyder, and S. Ryu, Classification of topological quantum matter with symmetries, [arXiv:1505.03535](https://arxiv.org/abs/1505.03535).
 - [4] F. Wilczek, Majorana returns, *Nat. Phys.* **5**, 614 (2009).
 - [5] M. Franz, Viewpoint: Race for Majorana fermions, *Physics* **3**, 24 (2010).
 - [6] J. Alicea, New directions in the pursuit of Majorana fermions in solid state systems, *Rep. Prog. Phys.* **75**, 076501 (2012).
 - [7] C. W. J. Beenakker, Search for Majorana Fermions in Superconductors, *Annu. Rev. Condens. Matter Phys.* **4**, 113 (2013).
 - [8] S. R. Elliott and M. Franz, Majorana fermions in nuclear, particle, and solid-state physics, *Rev. Mod. Phys.* **87**, 137 (2015).
 - [9] A. Yu Kitaev, Unpaired Majorana fermions in quantum wires, *Phys. Usp.* **44**, 131 (2001).
 - [10] M. Stone and R. Roy, Edge modes, edge currents, and gauge invariance in $p_x + ip_y$ superfluids and superconductors, *Phys. Rev. B* **69**, 184511 (2004).
 - [11] P. Fendley, M. P. A. Fisher, and C. Nayak, Edge states and tunneling of non-Abelian quasiparticles in the $\nu = 5/2$ quantum Hall state and $p_x + ip_y$ superconductors, *Phys. Rev. B* **75**, 045317 (2007).
 - [12] S. Tewari, S. Das Sarma, C. Nayak, C. Zhang, and P. Zoller, Quantum Computation using Vortices and Majorana Zero Modes of a $p_x + ip_y$ Superfluid of Fermionic Cold Atoms, *Phys. Rev. Lett.* **98**, 010506 (2007).
 - [13] S. Raghu, A. Kapitulnik, and S. A. Kivelson, Hidden Quasi-One-Dimensional Superconductivity in Sr_2RuO_4 , *Phys. Rev. Lett.* **105**, 136401 (2010).
 - [14] S. B. Chung, H.-J. Zhang, X.-L. Qi, and S.-C. Zhang, Topological superconducting phase and Majorana fermions in half-metal/superconductor heterostructures, *Phys. Rev. B* **84**, 060510(R) (2011).
 - [15] R. M. Lutchyn, J. D. Sau, and S. Das Sarma, Majorana Fermions and a Topological Phase Transition in Semiconductor-Superconductor Heterostructures, *Phys. Rev. Lett.* **105**, 077001 (2010).
 - [16] Y. Oreg, G. Refael, and F. von Oppen, Helical Liquids and Majorana Bound States in Quantum Wires, *Phys. Rev. Lett.* **105**, 177002 (2010).
 - [17] A. Cook and M. Franz, Majorana fermions in a topological-insulator nanowire proximity-coupled to an s -wave superconductor, *Phys. Rev. B* **84**, 201105(R) (2011).
 - [18] T. D. Stanescu and S. Tewari, Majorana fermions in semiconductor nanowires: fundamentals, modeling, and experiment, *J. Phys. Condens. Matter* **25**, 233201 (2013).
 - [19] S. Nadj-Perge, I. K. Drozdov, B. A. Bernevig, and A. Yazdani, Proposal for realizing Majorana fermions in chains of magnetic atoms on a superconductor, *Phys. Rev. B* **88**, 020407(R) (2013).
 - [20] S. Nadj-Perge, I. K. Drozdov, J. Li, H. Chen, S. Jeon, J. Seo, A. H. MacDonald, B. A. Bernevig, and A. Yazdani, Observation of Majorana fermions in ferromagnetic atomic chains on a superconductor, *Science* **346**, 602 (2014).
 - [21] H.-Y. Hui, P. M. R. Brydon, J. D. Sau, S. Tewari, and S. Das Sarma, Majorana fermions in ferromagnetic chains on the surface of bulk spin-orbit coupled s -wave superconductors, *Sci. Rep.* **5**, 8880 (2015).
 - [22] E. Dumitrescu, B. Roberts, S. Tewari, J. D. Sau, and S. Das Sarma, Majorana fermions in chiral topological ferromagnetic nanowires, *Phys. Rev. B* **91**, 094505 (2015).
 - [23] L. Fu and C. L. Kane, Superconducting Proximity Effect and Majorana Fermions at the Surface of a Topological Insulator, *Phys. Rev. Lett.* **100**, 096407 (2008).
 - [24] J. Linder, Y. Tanaka, T. Yokoyama, A. Sudbø, and N. Nagaosa, Unconventional Superconductivity on a Topological Insulator, *Phys. Rev. Lett.* **104**, 067001 (2010).
 - [25] C.-K. Chiu, P. Ghaemi, and T. L. Hughes, Stabilization of Majorana Modes in Magnetic Vortices in the Superconducting Phase of Topological Insulators using Topologically Trivial Bands, *Phys. Rev. Lett.* **109**, 237009 (2012).
 - [26] H.-H. Hung, P. Ghaemi, T. L. Hughes, and M. J. Gilbert, Vortex lattices in the superconducting phases of doped topological insulators and heterostructures, *Phys. Rev. B* **87**, 035401 (2013).
 - [27] N. B. Kopnin and M. M. Salomaa, Mutual friction in superfluid $^3\text{He-B}$: Effects of bound states in the vortex core, *Phys. Rev. B* **44**, 9667 (1991).
 - [28] X.-L. Qi, T. L. Hughes, S. Raghu, and S.-C. Zhang, Time-Reversal-Invariant Topological Superconductors and Superfluids in Two and Three Dimensions, *Phys. Rev. Lett.* **102**, 187001 (2009).
 - [29] S. B. Chung and S.-C. Zhang, Detecting the Majorana Fermion Surface State of $^3\text{He-B}$ through Spin Relaxation, *Phys. Rev. Lett.* **103**, 235301 (2009).
 - [30] X.-J. Liu, L. Jiang, H. Pu, and H. Hu, Probing Majorana fermions in spin-orbit-coupled atomic Fermi gases, *Phys. Rev. A* **85**, 021603(R) (2012).
 - [31] C. Qu, Z. Zheng, M. Gong, Y. Xu, Li Mao, X. Zou, G. Guo, and C. Zhang, Topological superfluids with finite-momentum pairing and Majorana fermions, *Nat. Commun.* **4**, 2710 (2013).
 - [32] W. Zhang and W. Yi, Topological Fulde-Ferrell-Larkin-Ovchinnikov states in spin-orbit-coupled Fermi gases, *Nat. Commun.* **4**, 2711 (2013).
 - [33] C. Chen, Inhomogeneous Topological Superfluidity in One-Dimensional Spin-Orbit-Coupled Fermi Gases, *Phys. Rev. Lett.* **111**, 235302 (2013).
 - [34] J. Ruhman, E. Berg, and E. Altman, Topological States in a One-Dimensional Fermi Gas with Attractive Interaction, *Phys. Rev. Lett.* **114**, 100401 (2015).
 - [35] L. Jiang, C. Qu, and C. Zhang, 1D topological chains with Majorana fermions in 2D non-topological optical lattices, [arXiv:1503.01810](https://arxiv.org/abs/1503.01810).
 - [36] V. Mourik, K. Zuo, S. M. Frolov, S. R. Plissard, E. P. A. M. Bakkers, and L. P. Kouwenhoven, Signatures of Majorana Fermions in Hybrid Superconductor-Semiconductor Nanowire Devices, *Science* **336**, 1003 (2012).
 - [37] M. T. Deng, C. Yu, G. Huang, M. Larsson, P. Caroff, and H. Q. Xu, Anomalous Zero-Bias Conductance Peak in a Nb-InSb Nanowire-Nb Hybrid Device, *Nano Lett.* **12**, 6414 (2012).
 - [38] L. P. Rokhinson, X. Lui, and J. K. Furdyna, The fractional a.c. Josephson effect in a semiconductor-superconductor nanowire as a signature of Majorana particles, *Nat. Phys.* **8**, 795 (2012).
 - [39] A. Das, Y. Ronen, Y. Most, Y. Oreg, M. Heiblum, and H. Shtrikman, Zero-bias peaks and splitting in an Al-InAs nanowire topological superconductor as a signature of Majorana fermions, *Nat. Phys.* **8**, 887 (2012).

- [40] A. D. K. Finck, D. J. Van Harlingen, P. K. Mohseni, K. Jung, and X. Li, Anomalous Modulation of a Zero-Bias Peak in a Hybrid Nanowire-Superconductor Device, *Phys. Rev. Lett.* **110**, 126406 (2013).
- [41] H. O. H. Churchill, V. Fatemi, K. Grove-Rasmussen, M. T. Deng, P. Caroff, H. Q. Xu, and C. M. Marcus, Superconductor-nanowire devices from tunneling to the multichannel regime: Zero-bias oscillations and magnetoconductance crossover, *Phys. Rev. B* **87**, 241401(R) (2013).
- [42] C. J. Bolech and E. Demler, Observing Majorana bound States in p -Wave Superconductors Using Noise Measurements in Tunneling Experiments, *Phys. Rev. Lett.* **98**, 237002 (2007).
- [43] K. T. Law, P. A. Lee, and T. K. Ng, Majorana Fermion Induced Resonant Andreev Reflection, *Phys. Rev. Lett.* **103**, 237001 (2009).
- [44] C. Qu, Y. Zhang, Li Mao, and C. Zhang, Signature of Majorana Fermions in Charge Transport in Semiconductor Nanowires, [arXiv:1109.4108](https://arxiv.org/abs/1109.4108).
- [45] J. Liu, A. C. Potter, K. T. Law, and P. A. Lee, Zero-Bias Peaks in the Tunneling Conductance of Spin-Orbit-Coupled Superconducting Wires With and Without Majorana End-States, *Phys. Rev. Lett.* **109**, 267002 (2012).
- [46] C.-H. Lin, J. D. Sau, and S. Das Sarma, Zero-bias conductance peak in Majorana wires made of semiconductor/superconductor hybrid structures, *Phys. Rev. B* **86**, 224511 (2012).
- [47] D. Roy, C. J. Bolech, and N. Shah, Majorana fermions in a topological superconducting wire out of equilibrium: Exact microscopic transport analysis of a p -wave open chain coupled to normal leads, *Phys. Rev. B* **86**, 094503 (2012); Nature of the zero-bias conductance peak associated with Majorana bound states in topological phases of semiconductor-superconductor hybrid structures, [arXiv:1303.7036](https://arxiv.org/abs/1303.7036).
- [48] Ph. Jacquod and M. Büttiker, Signatures of Majorana fermions in hybrid normal-superconducting rings, *Phys. Rev. B* **88**, 241409(R) (2013).
- [49] D. E. Liu, Proposed Method for Tunneling Spectroscopy with Ohmic Dissipation Using Resistive Electrodes: A Possible Majorana Filter, *Phys. Rev. Lett.* **111**, 207003 (2013).
- [50] S.-W. Li, Z.-Z. Li, C. Y. Cai, and C. P. Sun, Probing zero modes of a defect in a Kitaev quantum wire, *Phys. Rev. B* **89**, 134505 (2014).
- [51] B. H. Wu, W. Yi, J. C. Cao, and G.-C. Guo, Noncollinear Andreev reflections in semiconductor nanowires, *Phys. Rev. B* **90**, 205435 (2014).
- [52] R. J. Doornenbal, G. Skantzaris, and H. T. C. Stoof, Conductance of a finite Kitaev chain, *Phys. Rev. B* **91**, 045419 (2015).
- [53] F. Setiawan, P. M. R. Brydon, J. D. Sau, and S. Das Sarma, Conductance spectroscopy of topological superconductor wire junctions, *Phys. Rev. B* **91**, 214513 (2015).
- [54] P. L. S. Lopes, Pouyan Ghaemi, Magnification of signatures of a topological phase transition by quantum zero point motion, *Phys. Rev. B* **92**, 064518 (2015).
- [55] E. J. H. Lee, X. Jiang, R. Aguado, G. Katsaros, C. M. Lieber, and S. De Franceschi, Zero-Bias Anomaly in a Nanowire Quantum Dot Coupled to Superconductors, *Phys. Rev. Lett.* **109**, 186802 (2012).
- [56] G. Kells, D. Meidan, and P. W. Brouwer, Near-zero-energy end states in topologically trivial spin-orbit coupled superconducting nanowires with a smooth confinement, *Phys. Rev. B* **86**, 100503(R) (2012).
- [57] K. Sun and N. Shah, General framework for transport in spin-orbit-coupled superconducting heterostructures: Nonuniform spin-orbit coupling and spin-orbit-active interfaces, *Phys. Rev. B* **91**, 144508 (2015).
- [58] D. Bercioux and P. Lucignano, Quantum transport in Rashba spin-orbit materials: A review, [arXiv:1502.00570](https://arxiv.org/abs/1502.00570).
- [59] S. M. A. Rombouts, J. Dukelsky, and G. Ortiz, Quantum phase diagram of the integrable $p_x + ip_y$ fermionic superfluid, *Phys. Rev. B* **82**, 224510 (2010).
- [60] K. Sun, C.-K. Chiu, H.-H. Hung, and J. Wu, Tuning between singlet, triplet, and mixed pairing states in an extended Hubbard chain, *Phys. Rev. B* **89**, 104519 (2014).
- [61] A. Amaricci, J. C. Budich, M. Capone, B. Trauzettel, and G. Sangiovanni, First-Order Character and Observable Signatures of Topological Quantum Phase Transitions, *Phys. Rev. Lett.* **114**, 185701 (2015).
- [62] E. M. Stoudenmire, J. Alicea, O. A. Starykh, and M. P. A. Fisher, Interaction effects in topological superconducting wires supporting Majorana fermions, *Phys. Rev. B* **84**, 014503 (2011).
- [63] R. Thomale, S. Rachel, and P. Schmitteckert, Tunneling spectra simulation of interacting Majorana wires, *Phys. Rev. B* **88**, 161103(R) (2013).
- [64] F. Lin and V. W. Scarola, Enhancing the Thermal Stability of Majorana Fermions with Redundancy Using Dipoles in Optical Lattices, *Phys. Rev. Lett.* **111**, 220401 (2013).
- [65] G. Ortiz, J. Dukelsky, E. Cobanera, C. Esebbag, and C. Beenakker, Many-Body Characterization of Particle-Conserving Topological Superfluids, *Phys. Rev. Lett.* **113**, 267002 (2014).
- [66] Y.-H. Chan, Numerical analysis of spin-orbit-coupled one-dimensional Fermi gas in a magnetic field, *Phys. Rev. B* **91**, 235136 (2015).
- [67] A. Keselman and E. Berg, Gapless symmetry-protected topological phase of fermions in one dimension, *Phys. Rev. B* **91**, 235309 (2015).
- [68] E. Sela, A. Altland, and A. Rosch, Majorana fermions in strongly interacting helical liquids, *Phys. Rev. B* **84**, 085114 (2011).
- [69] F. Hassler and D. Schuricht, Strongly interacting Majorana modes in an array of Josephson junctions, *New J. Phys.* **14**, 125018 (2012).
- [70] H.-H. Hung, L. Wang, Z.-C. Gu, and G. A. Fiete, Topological phase transition in a generalized Kane-Mele-Hubbard model: A combined quantum Monte Carlo and Green's function study, *Phys. Rev. B* **87**, 121113(R) (2013); H.-H. Lai and H.-H. Hung, Effects of short-ranged interactions on the Kane-Mele model without discrete particle-hole symmetry, *Phys. Rev. B* **89**, 165135 (2014); H.-H. Hung, V. Chua, L. Wang, and G. A. Fiete, Interaction effects on topological phase transitions via numerically exact quantum Monte Carlo calculations, *Phys. Rev. B* **89**, 235104 (2014); H.-H. Lai, H.-H. Hung, and G. A. Fiete, Short-ranged interaction effects on Z_2 topological phase transitions, *Phys. Rev. B* **90**, 195120 (2014).
- [71] L. Fidkowski and A. Kitaev, Effects of interactions on the topological classification of free fermion systems, *Phys. Rev. B* **81**, 134509 (2010); Topological phases of

- fermions in one dimension, *Phys. Rev. B* **83**, 075103 (2011).
- [72] G. Goldstein and C. Chamon, Exact zero modes in closed systems of interacting fermions, *Phys. Rev. B* **86**, 115122 (2012).
- [73] G. Kells, Many-body Majorana operators and the equivalence of parity sectors, *Phys. Rev. B* **92**, 081401(R) (2015); Multi-particle content of Majorana zero-modes in the interacting p-wave wire, [arXiv:1507.06539](#).
- [74] A. Yu Kitaev, Fault-tolerant quantum computation by anyons, *Ann. Phys.* **303**, 2 (2003).
- [75] C. Nayak, S. H. Simon, A. Stern, M. Freedman, and S. Das Sarma, Non-Abelian anyons and topological quantum computation, *Rev. Mod. Phys.* **80**, 1083 (2008).
- [76] J. Alicea, Y. Oreg, G. Refael, F. von Oppen, and M. P. A. Fisher, Non-Abelian statistics and topological quantum information processing in 1D wire networks, *Nat. Phys.* **7**, 412 (2011).
- [77] C. Laflamme, M. A. Baranov, P. Zoller, and C. V. Kraus, Hybrid topological quantum computation with Majorana fermions: A cold-atom setup, *Phys. Rev. A* **89**, 022319 (2014).
- [78] D. Nozadze and N. Trivedi, Compressibility as a probe of quantum phase transitions in topological superconductors, [arXiv:1504.00013](#).
- [79] S. R. White, Density matrix formulation for quantum renormalization groups, *Phys. Rev. Lett.* **69**, 2863 (1992); Density-matrix algorithms for quantum renormalization groups, *Phys. Rev. B* **48**, 10345 (1993).
- [80] U. Schollwöck, The density-matrix renormalization group *Rev. Mod. Phys.* **77**, 259 (2005).
- [81] L. Fidkowski, Entanglement Spectrum of Topological Insulators and Superconductors, *Phys. Rev. Lett.* **104**, 130502 (2010).
- [82] A. M. Turner, F. Pollmann, and E. Berg, Topological phases of one-dimensional fermions: An entanglement point of view, *Phys. Rev. B* **83**, 075102 (2011).
- [83] J. Borchmann, A. Farrell, S. Matsuura, and T. Pereg-Barnea, Entanglement spectrum as a probe for the topology of a spin-orbit-coupled superconductor, *Phys. Rev. B* **90**, 235150 (2014).
- [84] C. N. Yang, Concept of Off-Diagonal Long-Range Order and the Quantum Phases of Liquid He and of Superconductors, *Rev. Mod. Phys.* **34**, 694 (1962).
- [85] A. J. Leggett, *Quantum Liquids*, 1st ed. (Oxford University Press, Oxford, 2006).
- [86] O. Penrose and L. Onsager, Bose-Einstein Condensation and Liquid Helium, *Phys. Rev.* **104**, 576 (1956).
- [87] K. Sun, C. Lannert, and S. Vishveshwara, Probing condensate order in deep optical lattices, *Phys. Rev. A* **79**, 043422 (2009).
- [88] N. Read and D. Green, Paired states of fermions in two dimensions with breaking of parity and time-reversal symmetries and the fractional quantum Hall effect, *Phys. Rev. B* **61**, 10267 (2000).
- [89] H. Katsura, D. Schuricht, M. Takahashi, Exact ground states and topological order in interacting Kitaev/Majorana chains, [arXiv:1507.04444](#).
- [90] F. Iemini, L. Mazza, D. Rossini, R. Fazio, and D. Diehl, Localized Majorana-like modes in a number conserving setting: An exactly solvable model, [arXiv:1504.04230](#).
- [91] C. V. Kraus, M. Dalmonte, M. A. Baranov, A. M. Läuchli, and P. Zoller, Majorana Edge States in Atomic Wires Coupled by Pair Hopping, *Phys. Rev. Lett.* **111**, 173004 (2013).
- [92] J. Liang, X. Zhou, P. H. Chui, K. Zhang, S.-J. Gu, M. Gong, G. Chen, and S. Jia, Spin-orbit coupling induced unconventional pairings in a one-dimensional lattice, [arXiv:1404.3009](#); X. Zhou, K. Zhang, J. Liang, G. Chen, and S. Jia, Spin-orbit coupled repulsive Fermi atoms in a one-dimensional optical lattice, [arXiv:1501.07004](#).
- [93] P. W. Brouwer, M. Duckheim, A. Romito, and F. von Oppen, Topological superconducting phases in disordered quantum wires with strong spin-orbit coupling, *Phys. Rev. B* **84**, 144526 (2011).
- [94] A. M. Lobos, R. M. Lutchyn, and S. Das Sarma, Interplay of Disorder and Interaction in Majorana Quantum Wires, *Phys. Rev. Lett.* **109**, 146403 (2012).
- [95] W. DeGottardi, D. Sen, and S. Vishveshwara, Majorana Fermions in Superconducting 1D Systems Having Periodic, Quasiperiodic, and Disordered Potentials, *Phys. Rev. Lett.* **110**, 146404 (2013).
- [96] F. Créin, G. Zarándi, and P. Simon, Nonperturbative phase diagram of interacting disordered Majorana nanowires, *Phys. Rev. B* **90**, 121407(R) (2014).
- [97] P. Burset, F. Keidel, Y. Tanaka, N. Nagaosa, and B. Trauzettel, Transport signatures of superconducting hybrids with mixed singlet and chiral triplet states, *Phys. Rev. B* **90**, 085438 (2014).
- [98] X. Liu, J. D. Sau, and S. Das Sarma, Universal spin-triplet superconducting correlations of Majorana fermions, *Phys. Rev. B* **92**, 014513 (2015).
- [99] L. Fidkowski, R. M. Lutchyn, C. Nayak, and M. P. A. Fisher, Majorana zero modes in one-dimensional quantum wires without long-ranged superconducting order, *Phys. Rev. B* **84**, 195436 (2011).
- [100] S. S. Chung, K. Sun, and C. J. Bolech, Matrix product ansatz for Fermi fields in one dimension, *Phys. Rev. B* **91**, 121108(R) (2015).
- [101] J. H. H. Perk, H. W. Capel, Time-dependent xx-correlation functions in the one-dimensional XY-model, *Physica A* **89**, 265 (1977).
- [102] C. N. Yang and C. P. Yang, One-Dimensional Chain of Anisotropic Spin-Spin Interactions. I. Proof of Bethe's Hypothesis for Ground State in a Finite System, *Phys. Rev.* **150**, 321 (1966); One-Dimensional Chain of Anisotropic Spin-Spin Interactions. II. Properties of the Ground-State Energy Per Lattice Site for an Infinite System, *Phys. Rev.* **150**, 327 (1966).
- [103] R. J. Baxter, *Exactly solved models in statistical mechanics*, Dover Publications (2008); A. Luther and I. Peschel, Calculation of critical exponents in two dimensions from quantum field theory in one dimension, *Phys. Rev. B* **12**, 3908 (1975).
- [104] B. Kaufman, Crystal Statistics. II. Partition Function Evaluated by Spinor Analysis, *Phys. Rev.* **76**, 1232 (1949); T. D. Schultz, D. C. Mattis, and E. H. Lieb, Two-Dimensional Ising Model as a Soluble Problem of Many Fermions, *Rev. Mod. Phys.* **36**, 856 (1964); D. Boyanovsky, Field theory of the two-dimensional Ising model: Conformal invariance, order and disorder, and bosonization, *Phys. Rev. B* **39**, 6744 (1989).